



Article

Laser Scanning Based Surface Flatness Measurement Using Flat Mirrors for Enhancing Scan Coverage Range

Fangxin Li ¹, **Heng Li** ¹, **Min-Koo Kim** ^{2,*} and **King-Chi Lo** ¹

¹ Department of Building and Real Estate, Hong Kong Polytechnic University, Kowloon, Hong Kong 999077, China; fangxin.li@connect.polyu.hk (F.L.); hengli.li@connect.polyu.hk (H.L.); king-chi-lo.lo@connect.polyu.hk (K.-C.L.)

² Department of Architectural Engineering, Chungbuk National University, Cheongju 28644, Korea

* Correspondence: joekim@chungbuk.ac.kr

Abstract: Surface flatness is an important indicator for the quality assessment of concrete surfaces during and after slab construction in the construction industry. Thanks to its speed and accuracy, terrestrial laser scanning (TLS) has been popularly used for surface flatness inspection of concrete slabs. However, the current TLS based approach for surface flatness inspection has two primary limitations associated with scan range and occluded area. First, the areas far away from the TLS normally suffer from inaccurate measurement caused by low scan density and high incident angle of laser beams. Second, physical barriers such as interior walls cause occluded areas where the TLS is not able to scan for surface flatness inspection. To address these limitations, this study presents a new method that employs flat mirrors to increase the measurement range with acceptable measurement accuracy and make possible the scanning of occluded areas even when the TLS is out of sight. To validate the proposed method, experiments on two laboratory-scale specimens are conducted, and the results show that the proposed approach can enlarge the scan range from 5 m to 10 m. In addition, the proposed method is able to address the occlusion problem of the previous methods by changing the laser beam direction. Based on these results, it is expected that the proposed technique has the potential for accurate and efficient surface flatness inspection in the construction industry.



Citation: Li, F.; Li, H.; Kim, M.-K.; Lo, K.-C. Laser Scanning Based Surface Flatness Measurement Using Flat Mirrors for Enhancing Scan Coverage Range. *Remote Sens.* **2021**, *13*, 714. <https://doi.org/10.3390/rs13040714>

Received: 19 January 2021

Accepted: 7 February 2021

Published: 15 February 2021

Publisher's Note: MDPI stays neutral with regard to jurisdictional claims in published maps and institutional affiliations.



Copyright: © 2021 by the authors. Licensee MDPI, Basel, Switzerland. This article is an open access article distributed under the terms and conditions of the Creative Commons Attribution (CC BY) license (<https://creativecommons.org/licenses/by/4.0/>).

1. Introduction

Surface flatness is essential for dimensional quality inspection of construction elements and floors both during and after the manufacturing and construction stages in the construction industry [1–4]. This is because concrete surfaces with unacceptable deviations exceeding their specific tolerances may adversely affect both aesthetic and functional performances of the structure [3,5,6]. In addition, non-flat concrete surfaces may result in a poor connection between adjacent construction elements, leading to long term structural problems [3]. For these reasons, it is necessary to conduct a surface flatness inspection to evaluate the flatness quality of the target structure. Currently, the surface flatness of concrete surfaces is commonly measured using straightedges or the F-numbers method in the construction industry [2,7]. As for the straightedge approach, inspectors use a 10 ft (3 m) long straightedge to assess surface flatness based on certain geometry patterns such as grid patterns to define the height deviation between the target surface and the straight-edge [2]. The F-numbers method measures the elevation differences between a pair of points sampled on the surface using inclinometers or longitudinal differential floor profilometers [7,8]. However, these two traditional flatness assessment methods are performed manually or by contact-type devices, which are time-consuming, labor-intensive and prone to human errors. As an alternative, terrestrial laser scanner (TLS) has been widely used and considered as a promising 3D data acquisition technology for concrete surface inspection

because of the nature of noncontact and accurate measurement [9–17]. Nevertheless, there are still limitations according to previous studies in order to ensure the feasibility of the TLS-based surface flatness inspection. To be specific, one issue is that areas far away from the TLS normally suffer from inaccurate measurement caused by low scan density and high incident angle of laser beams. Another issue is caused by physical barriers such as interior walls, which may generate occluded areas where the TLS is not able to scan for surface flatness inspection.

To address these limitations of the current laser scanning approaches, this study presents a mirror-aided laser scanning technique. This paper is organized as follows: First, research background, including current practices of surface flatness inspection and a literature review are presented in Section 2. Two hypotheses that the proposed method would bring about alternatives for current limitations are introduced in Section 3, followed by the experimental design for validating the hypotheses in Section 4. Key results and related discussions are presented in Sections 5 and 6. Finally, this paper ends with a summary and suggestions for further work in Section 7.

2. Research Background

2.1. Current Practices for Surface Flatness Inspection

Surface flatness, often called surface regularity, presents the deviations in elevation of the surfaces [1], as shown in Figure 1. There are two common methods widely used for surface flatness inspection, which are the straightedge method [2] and the F-numbers method [2,7].

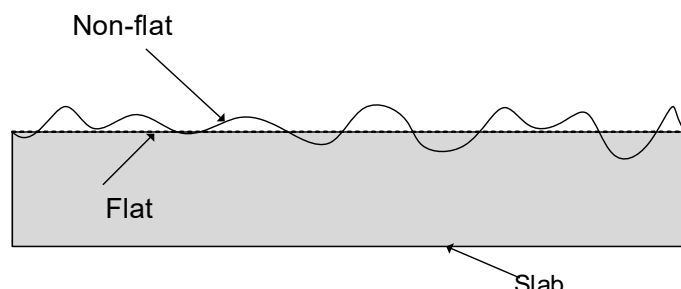


Figure 1. Illustration of flat and non-flat surfaces in the cross-section view of a slab.

As for the straightedge method [2], the primary steps are as follows. First, surveyors are required to randomly locate a straightedge with a length of 10 ft (3 m) at different locations on the surface. Then, the deviations of elevation between the straightedge and the surface are measured at the picked points using a stainless-steel slip. The deviations are then compared to the as-designed elevations to evaluate the surface flatness. Table 1 shows the tolerances of deviations in elevation using the straightedge method for concrete slabs specified in American Concrete Institute (ACI) 117 [2]. For example, the tolerance of 6 mm is specified for a concrete slab classified as “flat”. However, the straightedge method is performed manually and requires direct contact with the target surface, which is time-consuming and error-prone. In addition, there is no specification on the method of how to locate the straightedge on the surface, resulting in difficulties in practically implementing the method.

On the other hand, the F-numbers method [2,7] contains two ratings according to the ASTM E 1155 [7], which are floor flatness (F_F) numbers and floor levelness (F_L) numbers. The F_F numbers measure the degree to which a surface approximates a plane, whereas the F_L numbers depict the conformity of the floor surface to the intended slope indicated in the design documents. The F_F numbers method is discussed in the following since it measures the degree of flatness for a surface. Figure 2 illustrates the calculation of F_F numbers for surface flatness inspection [2]. First, sample measurement lines on the surface are created. Second, each sample measurement line is sampled into 300-mm long intervals, and the cut points are called “sample reading points”. Third, the elevations of the sample

points of the sample measurement lines are calculated. Note that the elevation of the sample points is presented by the height (z coordinate) of each scan point collected on the test surface. Finally, the F_F numbers, statistical numbers taking into account curvatures between all the sample points, are computed. Table 1 shows the flatness tolerances of concrete slabs specified in ACI 117 [2] for different flatness levels. Normally, a higher F_F number indicates a flatter surface. For example, a floor classified as “very flat” has an F_F number ranging from 35 to 45, while the F_F number of a floor regarded as “Conventional” is smaller than 20. Compared to the straightedge method, the F_F numbers method is advantageous in two aspects. First, the sample points are distributed throughout the whole surface as specified in the F_F numbers method, thereby covering and reflecting the elevation deviations globally. In addition, the interval of 300 mm between two sample points is much smaller compared to that of the straightedge method, resulting in a more accurate surface flatness measurement. For these reasons, the F_F numbers method is selected as the measurement of surface flatness in this study and the detailed steps are presented in Section 4.

Table 1. F_F numbers, its deviations of elevation and thresholds used for validation for 5 different types of concrete slabs specified in ACI 117 [2].

Surface Flatness Classification	Deviations of Elevation	F_F Numbers	Thresholds Used for Validation (20% of the Deviations of Elevation)
Conventional	13 mm	20	2.6 mm
Moderately flat	10 mm	25	2.0 mm
Flat	6 mm	35	1.2 mm
Very flat	5 mm	45	1.0 mm
Super flat	3 mm	60	0.6 mm

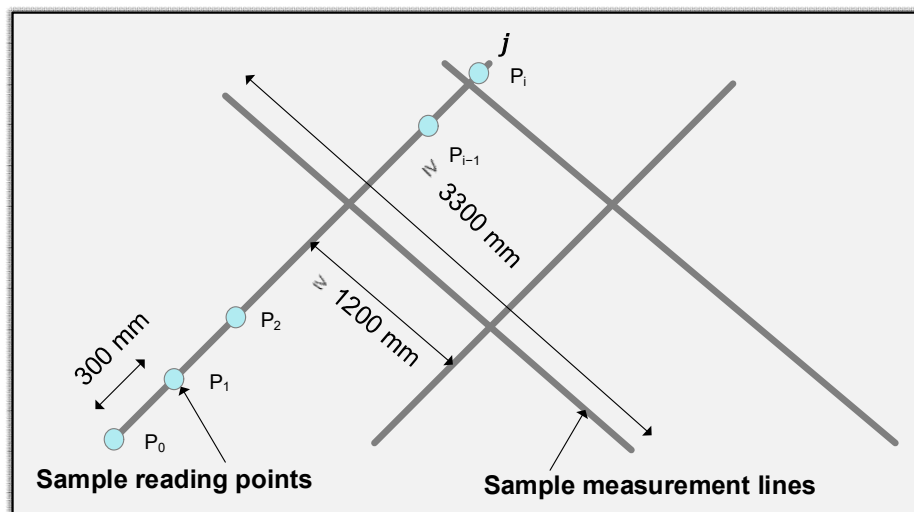


Figure 2. Illustration of determining F_F numbers on a slab.

Commercial TLSs normally have a measurement accuracy of around ± 3 mm within the measurement distance of 20 m [18]. Therefore, by adopting commercial TLSs, the laser scanning approach would not provide an accurate and robust flatness inspection for the flatness types of “very flat” and “super flat” due to the corresponding tolerances of deviations in elevation for the types being less than 6 mm according to Table 1. Therefore, one surface flatness type in this study, “conventional,” which has a deviation of 13 mm in elevation and F_F number of less than 20, is used to evaluate the applicability of the proposed mirror-aided approach. In addition, considering the measurement accuracy (± 3 mm) of the TLS used in this study, the estimation error of 20%, which is corresponding to 2.6 mm in deviations of elevation for the “conventional” surface type, is used as the

threshold to evaluate the effectiveness of the proposed method. In other words, it is classified as an “accurate” measurement if an estimation error is less than 20% compared to the ground-truth F_F number.

2.2. Surface Flatness Inspection Methods Using TLS

Several studies using TLS for the surface flatness inspection on floors and concrete slabs have been introduced. The previous studies can be divided into two categories: (1) surface flatness inspection following some guidelines such as the F-numbers method [19, 20] and (2) surface flatness inspection focusing on visual representation without following the standard documents to reflect surface flatness conditions [5,6,8,14,21].

As for the former type of studies using the guidelines, Bosché and Guenet [20] proposed an approach that compares an as-built model generated from a TLS with the as-designed model to inspect the surface flatness. In the study, the scanned data were first acquired and aligned with the as-designed model using the features of orthogonal distance and surface normal similarity. Then, the surface flatness was computed using the straight-edge method. The results showed a better performance of the TLS-based inspection in efficiency, reporting up to 50% inspection time compared to the manual-based method. Wang et al. [19] proposed a TLS-based surface flatness inspection approach for precast components based on the F_F numbers method. Experimental tests on two lab-scale specimens showed an estimation error of less than 8% in F_F numbers measurement. It was also found that the surface distortion, including warp and bowing, can deteriorate the accuracy of measurement of F_F numbers for surface flatness inspection. From the studies, it can be found that the TLS-based surface flatness inspection presents an efficient and accurate surface flatness inspection compared to manual-based methods. However, these studies are focused on simple structures, and there is no study investigating scan coverage of the TLS-based method. In addition, the occlusion problems caused by physical barriers such as interior walls have not been explored in these studies.

A large number of studies performing surface flatness inspection without standard guidelines have been proposed; Shih et al. [5] developed a technique to check the surface flatness of finished walls using a TLS. A plane generated from the collected point cloud data on the finished wall was first computed and set as a reference plane, and was followed by slicing the collected data per centimeter to visualize the flatness levels with different colors with respect to the reference plane. However, the method presented in the study used a one-centimeter size of slicing, which is too sparse to perform accurate surface flatness inspection on the finished wall. Li et al. [6] presented another study for slabs and floors. In the study, similar to [5], elevation deviations between each scan point and the fitted plane generated from the collected scan points were calculated, and a color-coded deviation map was then used to display the elevation deviations with different colors. Experimental studies conducted on an exterior wall panel showed that more than 80% of the scan points on the surface are within the allowable tolerance of 8 mm [22]. In contrast to the previous similar study [5] that measured the surface flatness with a relatively large slicing size of a centimeter, the study uses individual scan points to perform a more dense and accurate surface flatness inspection. However, the study lacks the investigation on the maximum area that can be covered by the proposed method for surface flatness inspection. Bosche and Biotteau [8] proposed a new method that processed point cloud data of concrete slabs in the frequency domain using the continuous wavelet transform (CWT) method [23]. Comparison tests between the CWT method and the waviness index (WI) method [24] were conducted, and it was found that the CWT method offers a more precise localization of non-flat areas of the concrete slabs due to its dense 3D measurement. However, the study utilizes the CWT method over multiple one-dimensional (1D)-survey lines from the cross-section view of the concrete slabs, which may not accurately reflect the actual flatness condition of the entire floor. To address the limitation of the study in [8], Puri et al. [21] proposed an approach that uses the CWT method in the two-dimensional (2D) domain instead of using a one-dimensional (1D) domain. Based on the comparison tests,

the 2D based CWT method was proved to perform better than the 1D based CWT method. However, the study only assesses the flatness accuracy without using ground-truth value; thus, the actual performance of the proposed method is not guaranteed. Lastly, Tang et al. [14] analyzed and compared three different algorithms for estimating concrete surface flatness deviations using point cloud data. Three algorithms, including range filtering, deviation filtering and sliding window, were formalized and implemented for surface flatness defect detection. The results showed that it is possible to detect surface flatness as small as 3 cm across and 1 mm thick with a scanning range of 20 m. However, the study lacks further investigation on the effects of scanning parameters, including incident angle and scanning distance, on the surface flatness inspection.

In summary, although the previous TLS-based surface flatness inspection shows potential for accurate and reliable surface flatness inspection compared to the contact-type manual practices, there are still limitations in two aspects. First, there has been no study on how far the laser scanning approach can cover the surface flatness inspection with acceptable measurement accuracy. Second, there have been few studies that discuss the limitation of occlusion problems, which inevitably occurred in the existence of physical barriers such as interior walls. To investigate such issues, this study presents a new approach that employs flat mirrors to increase the scan coverage range and enable flatness measurement even in occluded areas.

3. Research Hypotheses

This study proposes two hypotheses to enlarge the scanning range, increase the measurement accuracy in the long-range area far away from the TLS, and enable flatness measurement in hidden areas, as illustrated in Figure 3. Figure 3a illustrates hypothesis 1. Here, the scanning area far away from the TLS with a light gray color has a large scanning distance and a high incident angle (θ), resulting in a relatively low flatness measurement performance. With the implementation of the mirror-aided method, the laser beam emitted from the TLS is first reflected by the mirror and then reaches the long-range scanning area, leading to a lower incident angle (β) and higher surface flatness inspection accuracy. Since the study targets the front area on the basis of the mirror, the occluded areas behind the mirror are not considered. In addition, only virtual scan points generated by the mirror are used in this study due to the existence of a high incident angle problem for actual (direct) scan points, although the area under the mirror is scanned twice. With the help of using mirrors, the areas far from the TLS can be scanned with high accuracy, indicating that the proposed method can enlarge the scan range. Note that the long range area (marked as light gray color) is regarded as the enlarged area.

Note that there are rectangular patches attached to the surface of the flat mirror to be used for estimating the mirror plane using scan points falling onto the patches. Based on the mirror reflection principle [11], the scan points of the long-range area will be located on the virtual surface. In short, as the proposed method can have scan points with low incident angle, it can enlarge the scanning area and increase the surface flatness inspection efficiency. Figure 3b illustrates hypothesis 2 that the mirror-aided technique can address the occlusion problems caused by barriers. The construction elements such as the interior walls are likely to cause occlusion of the floor, which limits the scanning area of the TLS. Therefore, it requires multiple scans to perform the data collection, which deteriorates the surface flatness inspection efficiency. On the other hand, as the mirror can adjust the direction of the laser beam, the occlusion area of the floor can be scanned. Therefore, the mirror-aided approach can tackle the current limitation of the TLS-based surface flatness inspection.

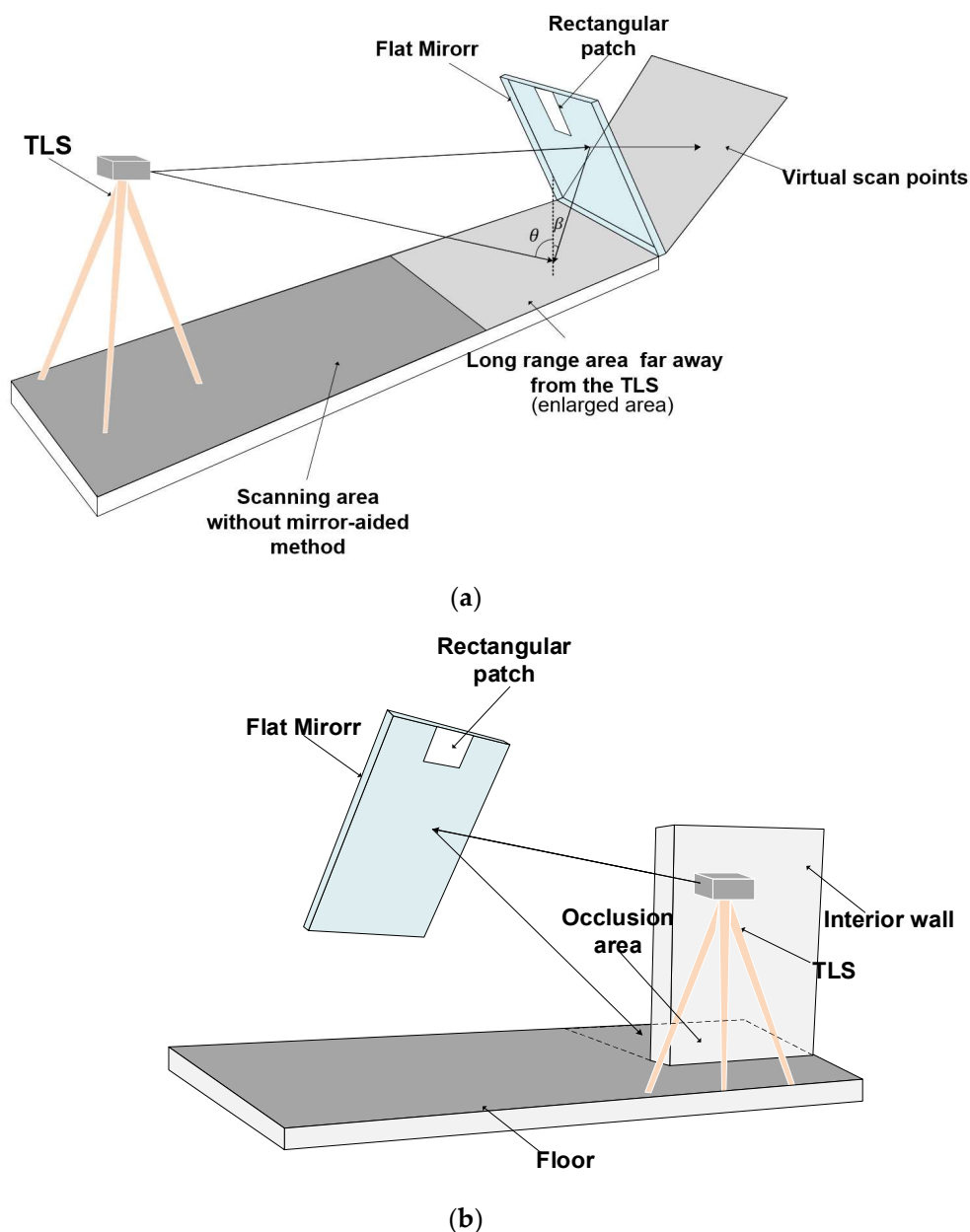


Figure 3. Illustration of the two hypotheses: (a) hypothesis 1—the proposed mirror-aided technique may increase scan coverage and inspection accuracy; and (b) hypothesis 2—the proposed mirror-aided technique may enable scanning of occlusion areas.

4. Experimental Configuration

4.1. Experimental Setup

Two experiments, named “experiment I” and “experiment II,” were conducted to validate the two hypotheses. The specific objectives of the experiments are to investigate: (1) the capability of the proposed mirror-aided approach to increase the surface flatness inspection accuracy at the areas far from the TLS and (2) the possibility of scanning occluded areas with an acceptable measurement accuracy with the existence of physical barriers for surface flatness inspection. Here, since there is no need to scan a large area of the surface for validating the accuracy at the far-field area, two lab-scale specimens were used in this study. Figure 4 shows the two specimens, named “specimen I” and “specimen II,” which are classified under the “conventional” flatness type. Table 2 illustrates the dimensions and F_F numbers of the specimens. The specimens were manufactured by a 3D printer,

ZRAPID iSLA880 [25], with the material of photopolymer resin. While specimen I has the dimensions of 400 mm (length) \times 400 mm (width) \times 10–23 mm (height) with the F_F number of 10.28, specimen II has the dimensions of 400 mm \times 400 mm \times 20–38 mm with the F_F number of 21.23. Note that according to ACI 117 [2], specimen II is designed to be flatter than specimen I.

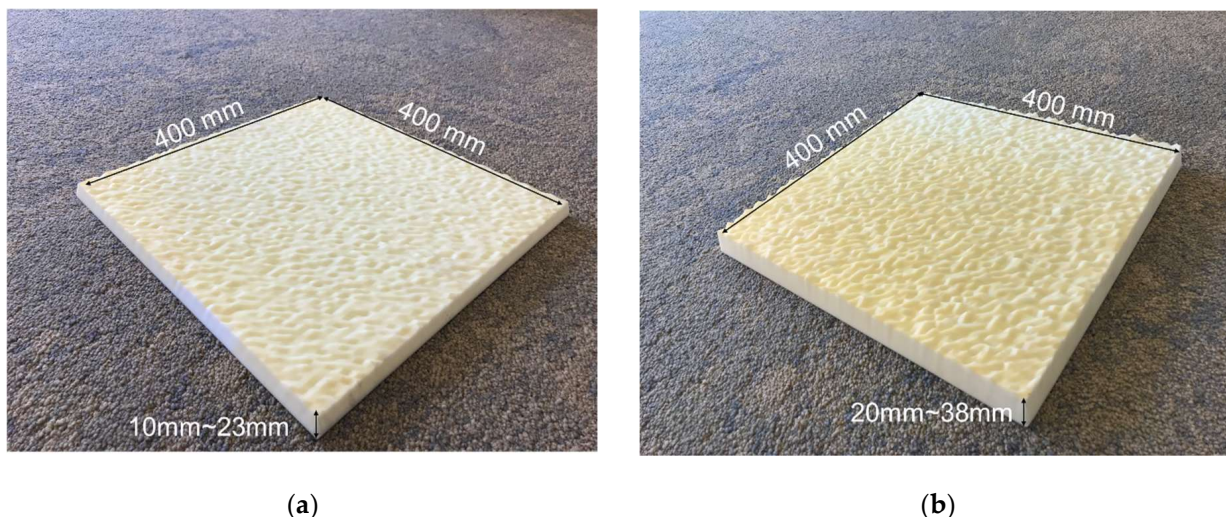


Figure 4. Two test specimens for validation: (a) specimen I with the F_F number of 10.28 and (b) specimen II with the F_F number of 21.23.

Table 2. Dimensions and F_F numbers of the specimens.

Items	Size (Length \times Width \times Height)	F_F Numbers
Specimen I	400 mm \times 400 mm \times 10–23 mm	10.28
Specimen II	400 mm \times 400 mm \times 20–38 mm	21.23

Figure 5 illustrates the test configuration of experiment I. A phase-shift TLS, FARO M70 [18], with a measurement error in distance deviation of ± 3 mm within scanning distance of 20 m, was used to acquire scan points of the specimen. The height distance of the TLS was set to 1.5 m, and the scanning distance was adjusted from 2.5 m to 12.5 m with an interval of 2.5 m in order to investigate the effects of the scanning distance on the accuracy of surface flatness inspection. Moreover, a flat mirror with the dimensions of 1000 mm (length) \times 1000 mm (height) was used to reflect laser beams to the specimens, and the flat mirror was located with a vertical angle of 75° to the ground for the laser beams to project a low incident angle on the surfaces of the two specimens. Furthermore, the mirror bottom line is located 0.5 m away from the backside of the specimen. In order to extract the mirror plane, two rectangular patches of 100 mm \times 100 mm were attached to the upper-side region of the mirrors. In addition, two different angular resolutions of 0.036° and 0.072° were employed for the tests.

Figure 6 shows the test configuration of experiment II. The TLS was set with a height of 2.5 m with respect to the ground and was located with a distance of 1.8 m and 1.2 m to the mirror and the specimen, respectively. Moreover, barriers were erected between the TLS and the specimen to create an environment that ensured that the specimen was invisible from the TLS. In addition, a mirror with the size of 1000 mm \times 1000 mm was located with a distance of 0.2 m behind the specimen. The mirror on the bottom line is set parallel to the specimen, positioned with a vertical angle of 70° with respect to the ground. As with experiment I, two rectangular patches of 100 mm \times 100 mm in size were attached to the upper-side region of the mirrors for mirror plane estimation, and two angular resolutions of 0.036° and 0.072° were used for the tests.

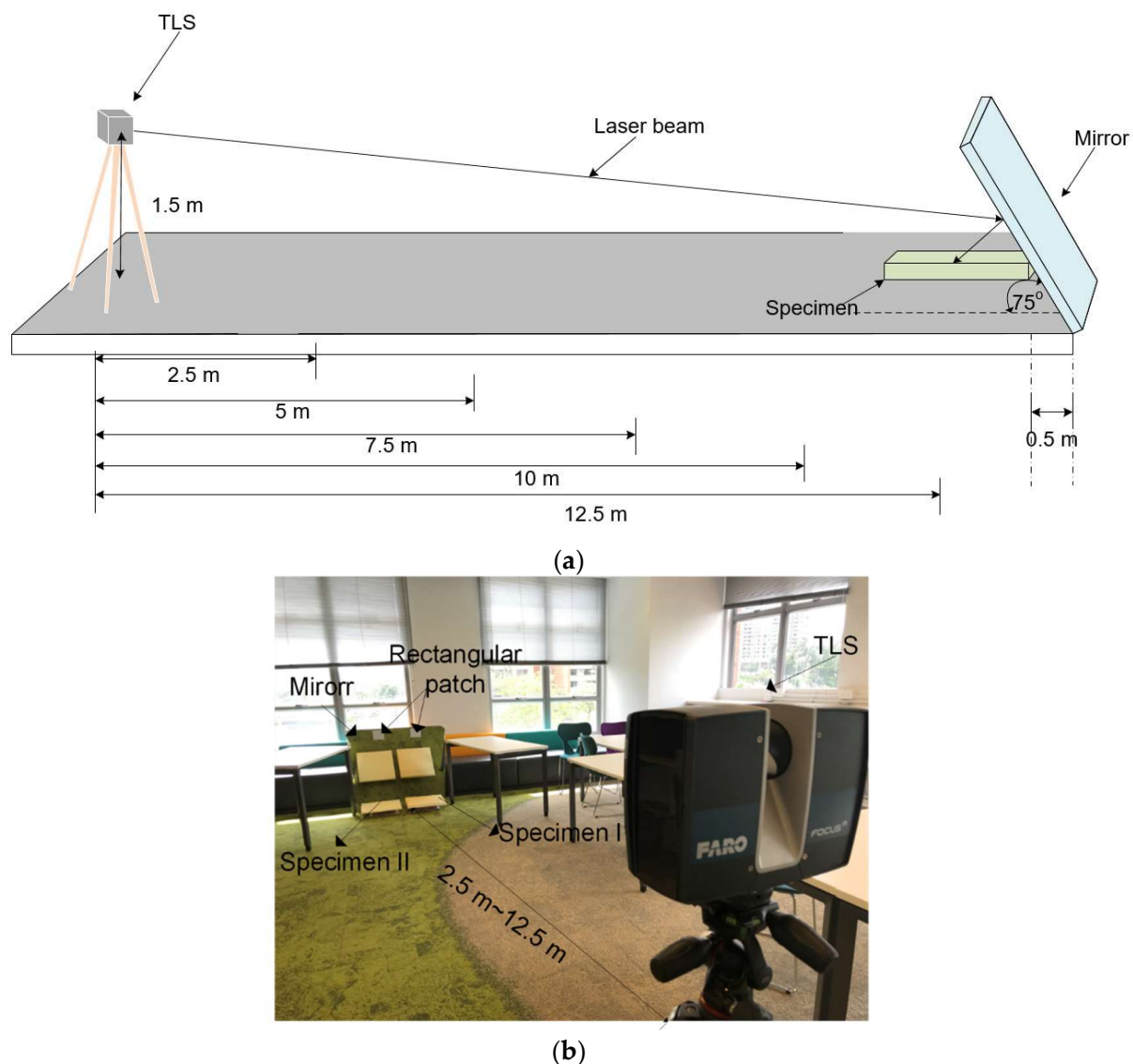


Figure 5. Test configuration of experiment I **(a)** side view of the test set up and **(b)** 3D view of the setup.

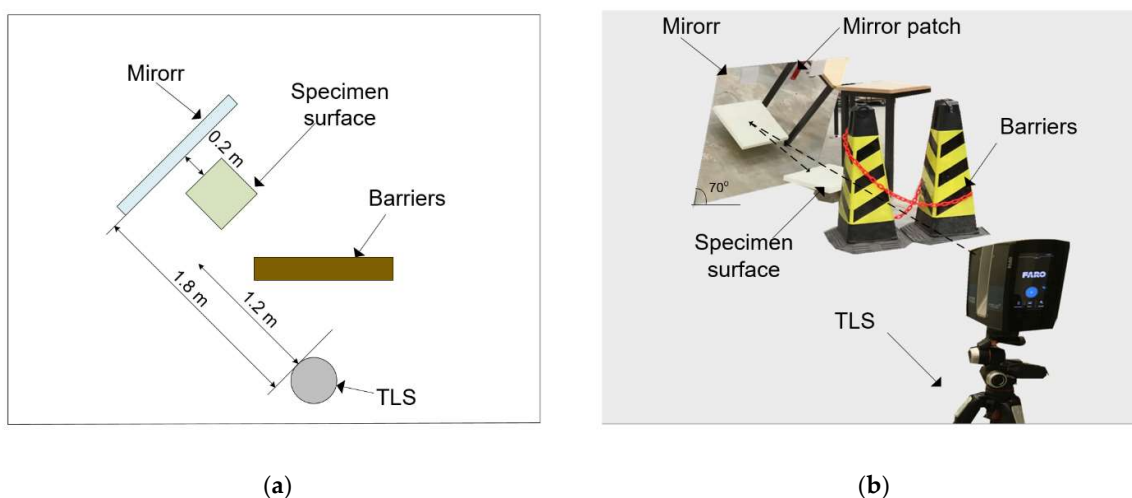


Figure 6. Test configuration of experiment II: **(a)** the top view of the setup and **(b)** a photo of the setup.

4.2. Data Processing

Data processing was composed of three steps: (1) data preprocessing, (2) virtual scan points transformation, and (3) surface flatness calculation. The details of each step are described in the following sections.

4.2.1. Data Preprocessing

This step aimed not only to remove background noise but also to extract the scan points of the specimens and rectangular patches attached to the mirror. Figure 7 shows the results. Note that there were three different types of raw scan data, including (1) background noise scan points, (2) specimen scan points and (3) rectangular patch scan points. It is worth noting that the background noise scan points contained two different noises, including ground noise and noise reflected by the mirror. To execute this data preprocessing step, the density-based spatial clustering of applications with noise (DBSCAN) algorithm [26] was first applied to the raw scan points to remove background noise based on the assumption that the scan data of the ground noise and noise reflected by the mirror were the two biggest clusters (named “1st” and “2nd” largest clusters) of the raw scan points as shown in Figure 7a. Next, after the removal of the background noise, the actual scan points and virtual scan points of the specimen were extracted and separated based on the assumptions that they become the 3rd and 4th largest scan clusters and the fitted plane of the actual scan points was nearly parallel to the ground plane. After this, the scan data sets corresponding to the rectangular patch attached to the mirror, extracted as the 5th largest cluster in the raw data, were finally classified.

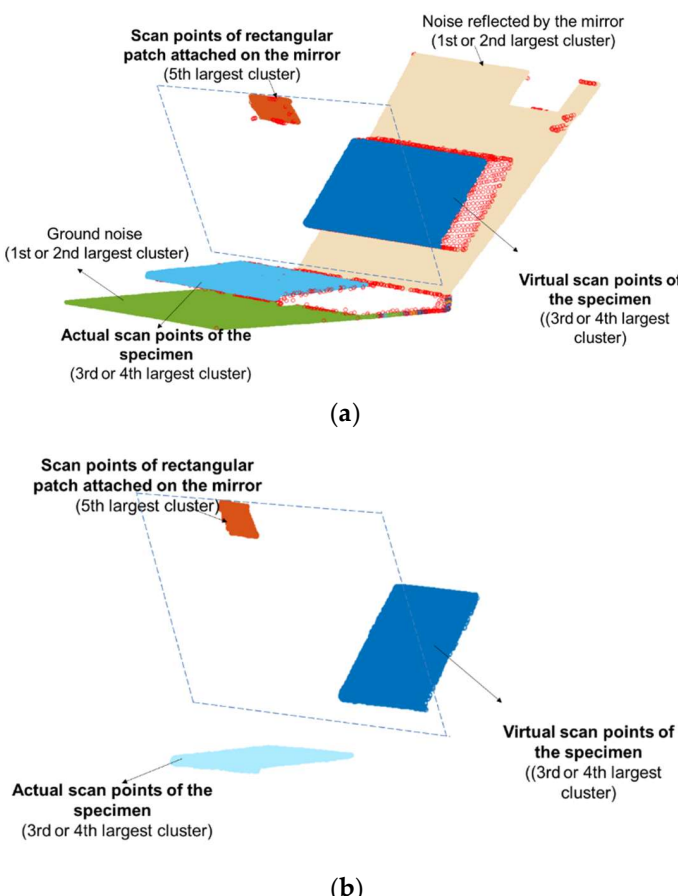


Figure 7. Data preprocessing results: (a) implementation result of the density-based spatial clustering of applications with noise (DBSCAN) on the raw scan points; and (b) extraction and separation of scan points corresponding to the specimen and the rectangular patch attached to the mirror.

4.2.2. Virtual Scan Points Transformation

This step aimed to transform the virtual scan points of the surface of the specimen to the position of the actual scan points. Here, the virtual scan points were transformed to the position of the actual scan points, which was parallel to the ground plane to facilitate the surface flatness inspection. Note that the virtual scan points collected from the mirror were compared with the actual scan points collected directly from the TLS to validate the effectiveness of the mirror-aided approach.

Due to the incompleteness of the DBSCAN algorithm, the extracted virtual scan points of the specimen contain outliers caused by the mixed pixels [27]. To remove the mixed-pixel outliers, the Random sample consensus (RANSAC) algorithm [28] was used, as shown in Figure 8a. Then, a mirror plane was estimated based on the scan points of the rectangular patches using the least fitting algorithm [29]. Once the mirror plane was generated, the virtual scan points of the top surface were finally transformed to the location of the actual scan points; this was based on the fact that the coordinates of the virtual and actual scan points were symmetric to each other with respect to the mirror plane. For each virtual scan point v (x_1, y_1, z_1), the 3D coordinates of the transformed scan point v' (x_2, y_2, z_2) was calculated using Equation (1). Note that A, B, C and D are the coefficients of the mirror plane and the transformed virtual scan points are shown in Figure 8b.

$$\begin{aligned}x_2 &= x_1 - \frac{2A(Ax_1+By_1+Cz_1+D)}{A^2+B^2+C^2} \\y_2 &= y_1 - \frac{2B(Ax_1+By_1+Cz_1+D)}{A^2+B^2+C^2} \\z_2 &= z_1 - \frac{2C(Ax_1+By_1+Cz_1+D)}{A^2+B^2+C^2}\end{aligned}\quad (1)$$

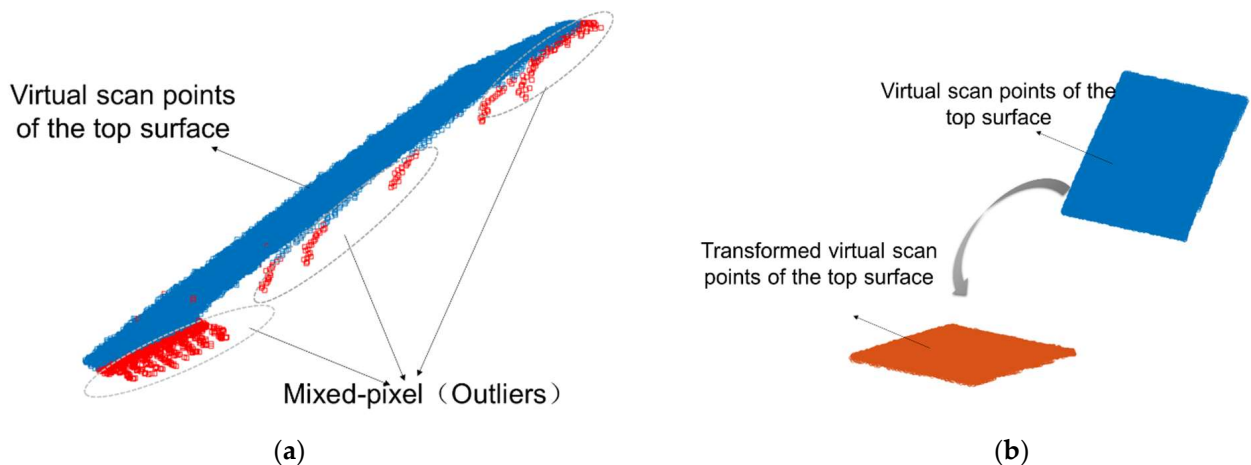


Figure 8. Transformation of the virtual scan points of the top surface on the specimen: (a) removal of the mixed-pixel outliers using the RANSAC algorithm and (b) transformation of the virtual scan points to the position of the actual scan points of the top surface of the specimen.

4.2.3. Surface Flatness Calculation

Once the virtual scan points transformation was conducted, the flatness of the specimen surface was then calculated using the F_F numbers method, as illustrated in Figure 2. The detailed procedure of computing the F_F numbers is presented in ASTM E 1155 [7].

5. Results

In order to investigate the feasibility of the proposed method based on the test results of experiment I, discrepancies between the ground-truth F_F numbers and the estimated F_F

numbers from the TLS are presented in Table 3. Note that as mentioned earlier in Section 2, the estimation error of 20%, which is equal to 2.6 mm in deviations of elevation, was used as the threshold in this study to assess the measurement performance of surface flatness. There are three distinctive findings as follows:

Table 3. Estimation errors for F_F numbers under varying angular resolutions and scanning distances.

Object	Scanning Distance (Incident Angle)	Estimation Error of F_F Numbers		Estimation Error of F_F Numbers	
		Specimen I in Percentage (Data Density: pts/cm ²)		Specimen II in Percentage (Data Density: pts/cm ²)	
		Angular Resolution	Angular Resolution	Angular Resolution	Angular Resolution
Virtual scan points	2.5 m (51°)	9.5% (87.7)	13.8% (21.9)	3.9% (87.2)	8.4% (21.9)
	5 m (43°)	9.6% (27.0)	11.1% (6.7)	4.0% (27.1)	19.1% (6.7)
	7.5 m (40°)	18.6% (12.7)	37.1% (3.2)	8.9% (12.9)	11.7% (3.2)
	10 m (38°)	15.1% (7.3)	49.0% (1.8)	19.8% (7.3)	23.3% (1.8)
Actual scan points	12.5 m (37°)	31.1% (4.9)	49.1% (1.2)	20.9% (4.8)	37.0% (1.2)
	2.5 m (70°)	19.9% (67.3)	36.1% (16.6)	4.4% (64.9)	27.0% (16.6)
	5 m (79°)	82.5% (10.6)	83.1% (2.7)	19.8% (10.6)	19.5% (2.5)
	7.5 m (82°)	161.4% (3.6)	140.5% (0.9)	58.7% (3.3)	88.4% (0.8)
Actual scan points	10 m (84°)	211.1% (1.5)	278.8% (0.4)	107.3% (1.4)	143.0% (0.3)
	12.5 m (86°)	210.3% (0.70)	−0.20	155.6% (0.60)	−0.20

First, virtual scan points collected from the mirror has a high estimation accuracy compared to actual scan points for both specimens I and II. Figure 9 shows the comparison results. It can be observed that the combination of long scanning range and large angular resolution yields high estimation errors that are larger than 20% in most cases. On the other hand, the F_F numbers estimation error for specimen I and specimen II are 20.5% and 12.4% on average within the distance of 10 m using the virtual scan points. This is because that the capability of the mirror can decrease the incident angle of laser beams to the ground by adjusting the vertical mirror angle. Therefore, scan density is increased due to the low incident angle of laser beams, resulting in the acquisition of large numbers of scan points. Therefore, it can be concluded that the proposed mirror-aided method can increase the flatness measurement accuracy in large distances.

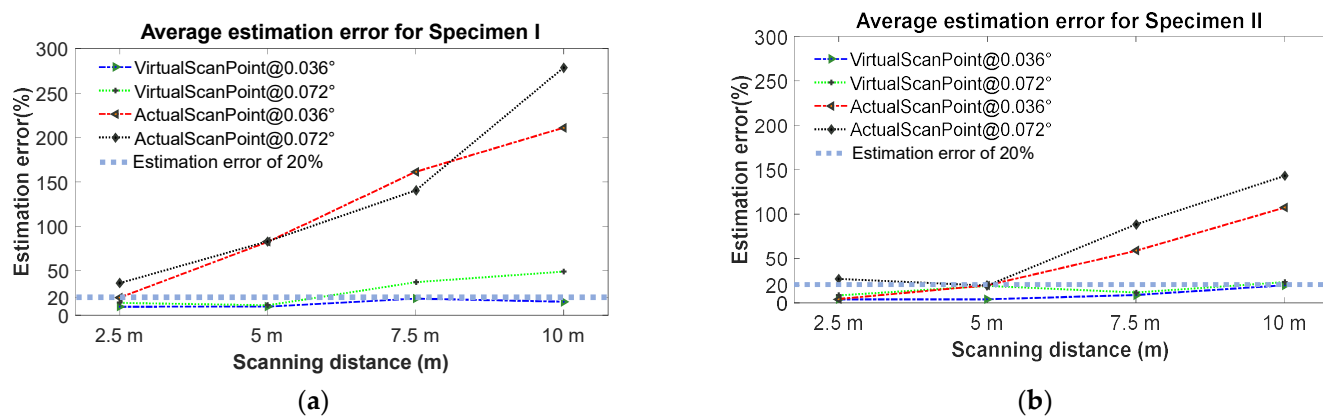


Figure 9. F_F number estimation errors under various angular resolutions and scanning distances: (a) average estimation error for specimen I and (b) average estimation error for specimen II.

Second, scan density largely affects the flatness measurement performance. Figure 10 shows the effect of scan density on the F_F number estimation errors. Note that the data density is defined as the number of scan points falling in the unit area of cm². One particular result shows that the estimation error is decreased from 211.1% to 3.9% as the scan density

increases from 0.3 pts/cm^2 to 87.7 pts/cm^2 . In addition, one noticeable observation is that the F_F numbers are unable to be computed in cases of the scan density being less than 0.2 pts/cm^2 . Considering the tolerance of 20% relative error set in this study, an accurate flatness measurement is assured when the target surface has a scan density of 6.7 pts/cm^2 . Therefore, the scan density should be checked to ensure an accurate surface flatness inspection.

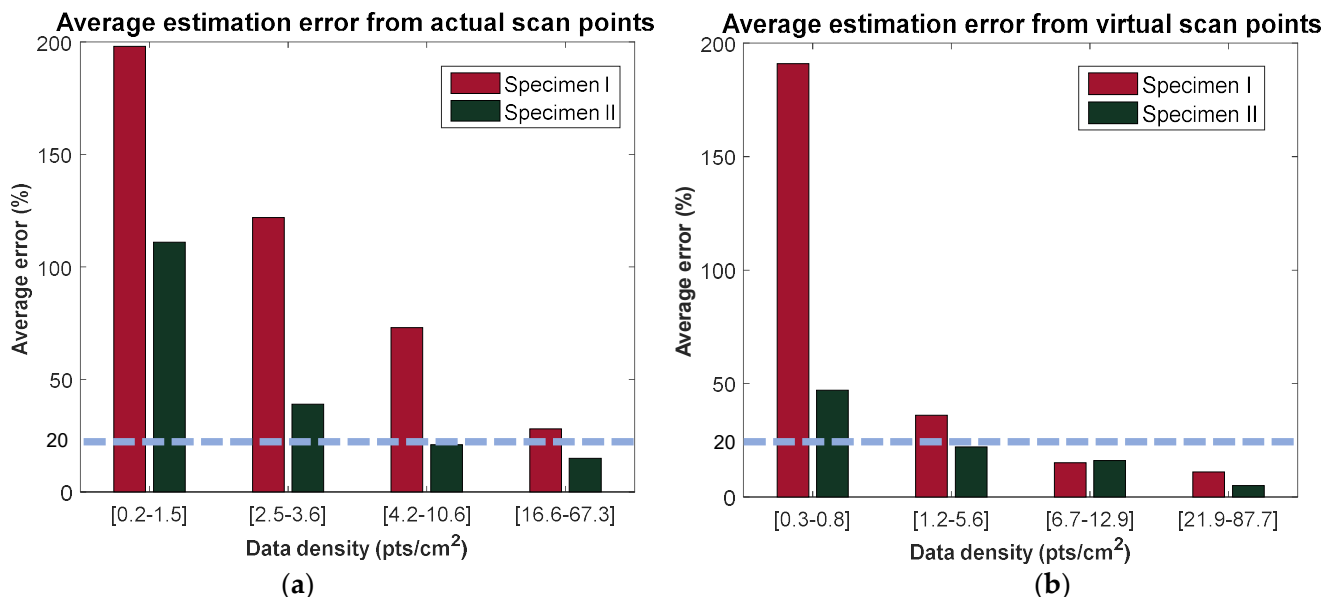


Figure 10. Estimation errors of F_F numbers with varying scan densities in specimen I and II: (a) average estimation error from actual scan points and (b) average estimation error from virtual scan points.

Third, specimen II achieves more accurate F_F number estimation results than specimen I in most cases, as shown in Figure 11, indicating that the mirror-aided approach is more robust for the flatness inspection of flatter surface. This phenomenon is caused by the fact that specimen I with a non-flat surface, as can be seen in Figure 4, is more likely to suffer from the effect of the high incident angle compared to specimen II with a relatively flatter surface. Normally, as common concrete surfaces of offices and laboratories are classified into “conventional”, which have similar F_F numbers as specimen II within the range from 20 to 25 [2], the proposed mirror-aided approach is expected to be effective for floor surface flatness inspection.

Regarding the test results of experiment II, Table 4 shows the mirror-aided F_F number estimation errors under varying angular resolutions. The average errors for specimen I and specimen II in percentage were 14.3% and 11.1%, respectively, demonstrating the applicability of the proposed mirror-aided method for hypothesis 2. This positive outcome is attributed to the fact that the mirror changes the laser beam direction to ensure that the occluded areas by the barrier are scanned. Similar to the results of experiment I, the F_F numbers estimation accuracy increased as the angular resolution decreases for both specimen I and specimen II due to the scan density effect. In addition, specimen II offers a more accurate F_F numbers estimation because the flatter surface of specimen II is more robust to the incident angle influence compared to the non-flatter surface of specimen I, which is similar to the results of experiment I. In summary, the mirror-aided approach was able to address the occlusion problem caused by construction elements such as interior walls.

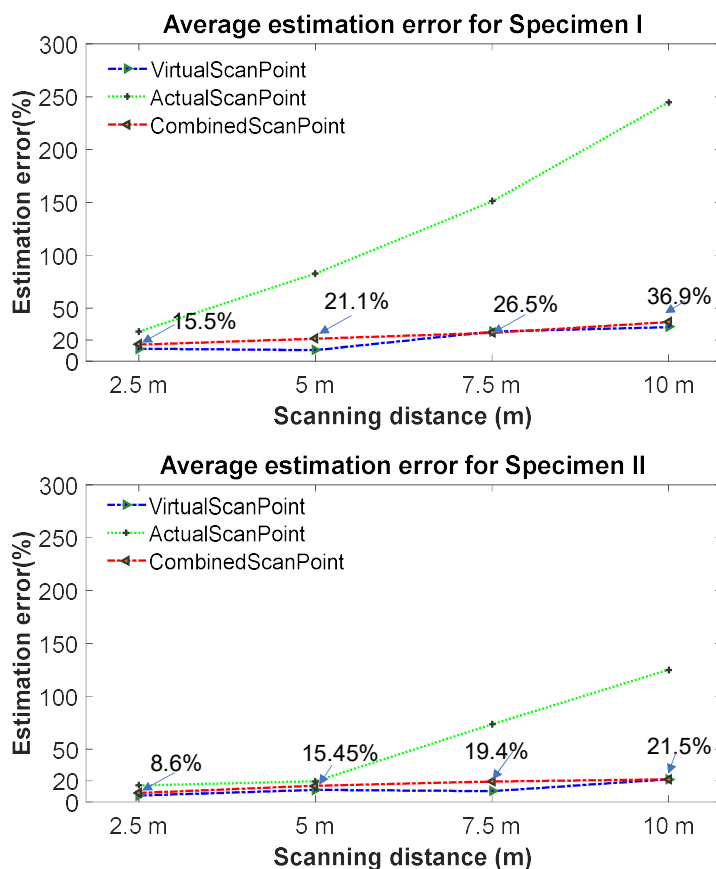


Figure 11. Comparison of F_F estimation errors among three types of scan points, including combined scan points, virtual scan points and actual scan points.

Table 4. F_F number estimation errors under varying angular resolutions for specimens with occlusion problem.

Object	F_F Numbers Estimation Error of Specimen I (mm)			F_F Numbers Estimation Error of Specimen II (mm)		
	Angular Resolution			Angular Resolution		
	0.036°	0.072°	Ave.	0.036°	0.072°	Ave.
Estimation error in percentage	10.7%	27.6%	14.3%	10.4%	11.8%	11.1%

6. Discussion

To further identify the effectiveness of the proposed method, further studies were conducted in two aspects, which are (1) investigation on the performance of combined scan points of actual and virtual scan points, and (2) determination of mirror location and mirror size for optimal surface flatness inspection.

6.1. Performance Comparison with Combined Scan Points

The actual scan points, which have a large incident angle and low scan density, can be merged with the virtual scan points to increase the scan density. For this reason, the actual scan points and virtual scan points are aligned together using an iterative closest point (ICP)-based algorithm [30]. Table 5 and Figure 11 shows the comparison results of scan density and F_F number estimation error of specimen I and II, respectively, with varying angular resolutions and scanning distances. A distinctive trend shows that using the virtual scan points exclusively shows the best performance of flatness inspection for the long-range area among the three different types of scan points, although the combined

scan points have the largest scan density of 34.0 pts/cm² and 33.6 pts/cm² for specimen I and specimen II, respectively. This phenomenon is attributed to the alignment errors of the ICP algorithm that deteriorates the F_F numbers estimation accuracy of the combined scan points. Therefore, it is suggested for construction engineers and inspectors to conduct surface flatness inspection directly using virtual scan points instead of combined scan points, although the combined scan points have a higher scan density.

Table 5. Scan density varying angular resolutions with different scanning distances of combined scan points, virtual scan points and actual scan points.

Object	Data Density of Specimen I (pts/cm ²)			Data Density of Specimen II (pts/cm ²)		
	Angular Resolution			Angular Resolution		
	0.036°	0.072°	Ave.	0.036°	0.072°	Ave.
Combined scan points	54.3	13.6	34.0	53.7	13.5	33.6
Virtual scan points	33.6	8.4	21.0	33.6	8.4	21.0
Actual scan points	20.7	5.2	13.0	20.1	5.1	12.6

6.2. Mirror Location and Mirror Size for Performing Surface Flatness Inspection

When applying the mirror-aided approach on sites, it is required to determine the mirror position and mirror. From the results stated in experiment I, a scan density of 6.7 pts/cm² was required to guarantee a successful flatness inspection. In addition, based on Figure 9a, the acceptable scanning range of TLS without the mirrors was limited to 5 m, while the mirror-aided approach was able to enlarge the scanning range up to 10 m. One issue when using the proposed method was that a large-scale mirror was necessary to scan the range between 5 m and 10 m. However, large-scale mirrors are fragile and cumbersome, so their usage is not optimal in manufacturing or construction environments. To tackle this limitation, a small-scale mirror that could rotate along the vertical axis could be used, as shown in Figure 12. Based on the geometrical relationship model developed in [31], the optimal mirror position, mirror size and mirror rotation angle R could be determined to cover the scan range between 5 m and 10 m.

Table 6 shows the results of the determination of the mirror rotation angle for the scan area between 5 m and 10 m. Figure 12 also shows the results in a side view. Assuming the height distance of the TLS as 1.5 m, a flat mirror with the dimensions of 1800 mm (length) was selected and positioned on the rotating axis for mirror rotation. Two mirror positions were determined at 7.5 m and 10 m away from the TLS, respectively, to cover the areas from 5 m to 10 m. Here, the positions of the two mirrors were 1.0 m and 2.0 m above the surface, respectively. As for the mirror located at 7.8 m away from the TLS, a mirror angle of 68° was determined to cover the area from 5.0 m to 7.8 m with a scan density of 8.2 pts/cm² on average. Moreover, as for the mirror located at 10 m away from the TLS, a rotation angle of 55° was computed as the optimal angle to had a scan density of 11.1 pts/cm². With the two mirrors, the scan area within the range of 10 m could be fully covered. In summary, the proposed mirror-aided approach has the potential for an accurate surface flatness inspection in the long-scan range. Even though the preparation of multiple mirrors is necessary for certain cases, the time cost is relatively small compared to the traditional method that inevitably involves several changes in scanner locations and selecting scan parameters for each scan position. In addition, registration errors that are normally problematic during the point cloud merging process did not occur in the proposed method due to the lack of a need to change the scanner location. Hence, the proposed scan planning is systemic optimization-oriented, which aims to ensure efficient data acquisition instead of generating extra work.

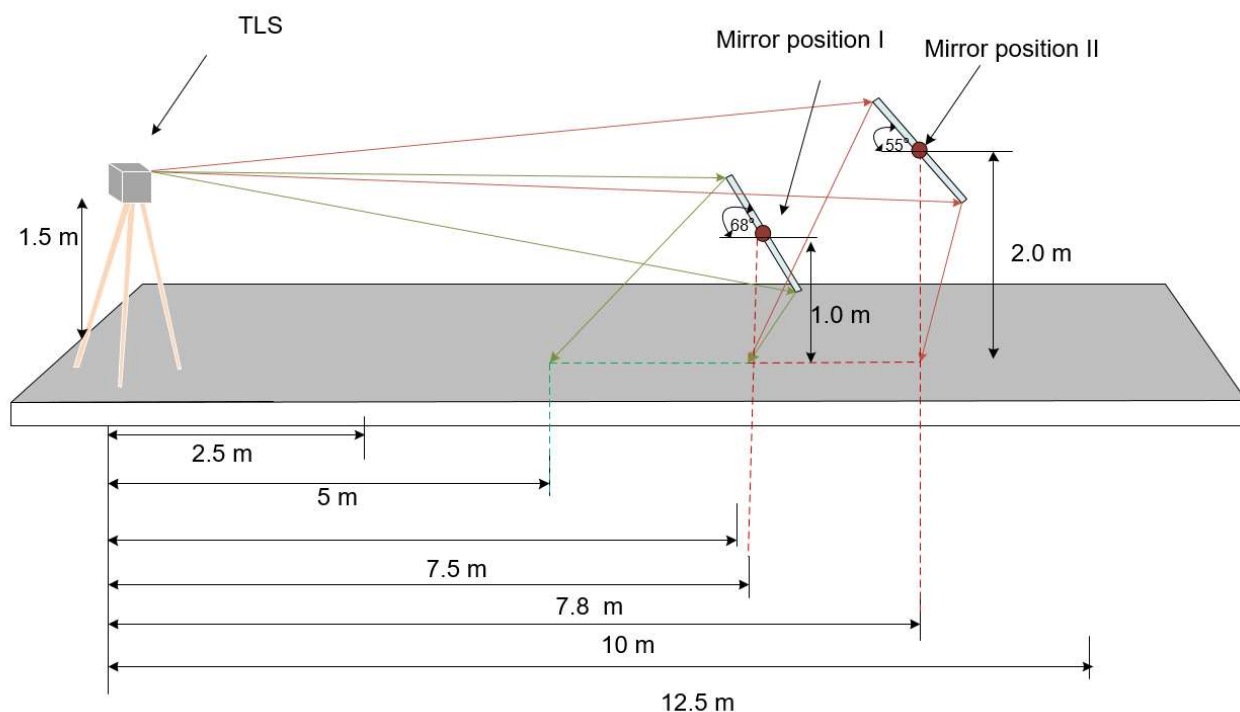


Figure 12. Determination of the mirror position, mirror size and mirror rotation angles for mirror-aided approach.

Table 6. Determination of the mirror rotation angle for the scan area to be enlarged.

Items	Determined Results	
	Mirror Position I	Mirror Position II
Mirror rotation angle	68°	55°
Scan coverage	5.0 m–7.8 m	7.8 m–10.0 m
Scan density	8.2 pts/cm ²	11.1 pts/cm ²

7. Conclusions

This study presents a mirror-aided technique for surface flatness inspection to address the low accuracy of the scanning area far from TLS and occlusion problems caused by barriers. In this study, two hypotheses are proposed for the mirror-aided surface flatness inspection method. First, the mirror-aided approach can increase the scan coverage range and increase the surface flatness inspection efficiency. Second, the mirror-aided approach can measure the flatness of the floors occluded by construction elements based on the mirror reflection principle with one single scan, resulting in efficient surface flatness inspection. To validate the two hypotheses, two experiments are conducted on two laboratory-scale specimens. The validation results indicate that the mirror-aided approach can adjust the incident angle of laser beams to address the low measurement caused by the low incident angle, enlarging the scan range from 5 m to 10 m. In addition, the mirror-aided approach is able to address the occlusion problem caused by construction elements such as interior walls with a measurement accuracy of more than 80% on the scanning area for surface flatness inspection. From the results, the proposed technique has the potential for accurate and efficient surface flatness inspections in the construction industry. As this study focuses on surface flatness measurement, the size of the target scene is regarded as the major concern instead of the shape and complexity. Since this method can cover the surface up to a scan range of 10 m from the TLS from the test results, the proposed mirror-aided method is suitable for small and medium-size projects such as surfaces of interior rooms. There are two main applications in real projects using the proposed surface flatness inspection method. First, for those surface areas with an edge line of less than 5 m, the proposed

method can improve the accuracy of surface flatness measurement by setting flat mirrors near the far-edge (5 m from the TLS) line because our method using the mirrors can reflect laser beams to have lower incident angles. Second, in the case of having more than 5 m, but less than 10 m scan range from the TLS, the proposed mirror-aided approach is able to enlarge the scanning range from 5 m to 10 m, which minimizes the number of scans. The contributions of the proposed technique are: (1) develop a mirror-aided technique that increases the measurement accuracy in a long-range area far away from the TLS and enable flatness measurement in hidden areas caused by physical barriers such as interior walls, and (2) validate the applicability of the mirror-aided flatness inspection technique through validation experiments.

However, limitations remain for further study in the near future. First, the proposed mirror-aided flatness inspection method is validated on lab-scale specimens. Further validations on the field-scale are required in order to increase the applicability of the proposed technique, which involves the utilization of the rotating mirror system and an appropriate selection of the mirror location. Second, regarding the difficulty in finding the right place for placing the rotating mirrors in the dynamic and clustered environment, this study assumes that the space to be scanned is clean and spacious enough to place the rotating mirrors. Therefore, further investigation on the real applicability of dynamic and clustered scenarios such as construction sites and industrial plants can be a future direction. In addition, the proposed mirror-aided approach can be applied to the 3D reconstruction of small-scale structures with complex geometries to minimize the number of scans.

Author Contributions: Conceptualization, F.L. and M.-K.K.; Methodology, F.L., H.L. and M.-K.K.; Validation, F.L., M.-K.K. and K.-C.L.; Writing—original draft, F.L. and M.-K.K.; Writing—review & editing, M.-K.K. and F.L. All authors have read and agreed to the published version of the manuscript.

Funding: This research was supported by Basic Science Research Program through the National Research Foundation of Korea (NRF) funded by the Ministry of Education (2016R1A6A3A03010355).

Conflicts of Interest: The authors declare no conflict of interest.

References

1. British Standards Institution (BSI). *BS 8204-Screeds, Bases and In Situ Flooring*; BSI: London, UK, 2009.
2. American Concrete Institute (ACI). *ACI 117-06-Specifications for Tolerances for Concrete Construction and Materials and Commentary*; ACI: Farmington Hills, MI, USA, 2006.
3. Hieber, D.G.; Wacker, J.M.; Eberhard, M.O.; Stanton, J.F. State-of-the-Art Report on Precast Concrete Systems for Rapid Construction of Bridges. Washington State Transportation Center. (No. WA-RD 594.1); 2005. Available online: <https://rosap.ntl.bts.gov>. (accessed on 20 August 2020).
4. American Concrete Institute (ACI). *ACI 302.1R-96 -Guide for Concrete Floor and Slab Construction*; ACI: Farmington Hills, MI, USA, 1997.
5. Shih, N.; Wang, P. Using Point Cloud to Inspect the Construction Quality of Wall Finish. In Proceedings of the 22nd eCAADe Conference, Copenhagen, Denmark, 15–18 September 2004; pp. 573–578. Available online: <http://cuminad.scix.net/data/works/att>. (accessed on 1 August 2020).
6. Li, D.; Liu, J.; Feng, L.; Zhou, Y.; Liu, P.; Chen, Y.F. Terrestrial laser scanning assisted flatness quality assessment for two different types of concrete surfaces. *Measurement* **2020**, *154*, 107436. [[CrossRef](#)]
7. American Society for Testing (ASTM). *ASTM E 1155-96-Standard Test Method for Determining FF Floor Flatness and FL Floor Levelness Numbers*; ASTM: West Conshohocken, PA, USA, 2008.
8. Bosché, F.; Biotteau, B. Terrestrial laser scanning and continuous wavelet transform for controlling surface flatness in construction—A first investigation. *Adv. Eng. Inform.* **2015**, *29*, 591–601. [[CrossRef](#)]
9. Kim, M.-K.; Wang, Q.; Li, H. Non-contact sensing based geometric quality assessment of buildings and civil structures: A review. *Autom. Constr.* **2019**, *100*, 163–179. [[CrossRef](#)]
10. Kim, M.-K.; Thedja, J.P.P.; Wang, Q. Automated dimensional quality assessment for formwork and rebar of reinforced concrete components using 3D point cloud data. *Autom. Constr.* **2020**, *112*, 103077. [[CrossRef](#)]
11. Kim, M.-K.; Wang, Q.; Yoon, S.; Sohn, H. A mirror-aided laser scanning system for geometric quality inspection of side surfaces of precast concrete elements. *Measurement* **2019**, *141*, 420–428. [[CrossRef](#)]
12. Wang, Q.; Tan, Y.; Mei, Z. Computational Methods of Acquisition and Processing of 3D Point Cloud Data for Construction Applications. *Arch. Comput. Methods Eng.* **2019**, *27*, 479–499. [[CrossRef](#)]

13. Kim, M.-K.; Sohn, H.; Chang, C.C. Localization and Quantification of Concrete Spalling Defects Using Terrestrial Laser Scanning. *J. Comput. Civ. Eng.* **2015**, *29*, 04014086. [[CrossRef](#)]
14. Tang, P.; Huber, D.; Akinci, B. Characterization of Laser Scanners and Algorithms for Detecting Flatness Defects on Concrete Surfaces. *J. Comput. Civ. Eng.* **2011**, *25*, 31–42. [[CrossRef](#)]
15. Yoo, M.; Ham, N. Productivity Analysis of Documentation Based on 3D Model in Plant Facility Construction Project. *Appl. Sci.* **2020**, *10*, 1126. [[CrossRef](#)]
16. Ham, N.; Lee, S.H. Empirical Study on Structural Safety Diagnosis of Large-Scale Civil Infrastructure Using Laser Scanning and BIM. *Sustainability* **2018**, *10*, 4024. [[CrossRef](#)]
17. Erdélyi, J.; Kopáčik, A.; Kyrinovič, P. Spatial Data Analysis for Deformation Monitoring of Bridge Structures. *Appl. Sci.* **2020**, *10*, 8731. [[CrossRef](#)]
18. FARO. Faro® Laser Scanner Focus. Available online: <https://www.faro.com/ensg/products/construction-bim/faro-laser-scanner-focus> (accessed on 20 August 2020).
19. Wang, Q.; Kim, M.-K.; Sohn, H.; Cheng, J.C. Surface flatness and distortion inspection of precast concrete elements using laser scanning technology. *Smart Struct. Syst.* **2016**, *18*, 601–623. [[CrossRef](#)]
20. Bosché, F.; Guenet, E. Automating surface flatness control using terrestrial laser scanning and building information models. *Autom. Constr.* **2014**, *44*, 212–226. [[CrossRef](#)]
21. Puri, N.; Valero, E.; Turkan, Y.; Bosché, F. Assessment of compliance of dimensional tolerances in concrete slabs using TLS data and the 2D continuous wavelet transform. *Autom. Constr.* **2018**, *94*, 62–72. [[CrossRef](#)]
22. C. Standard. GB50204-2015-Code for Acceptance of Construction Quality of Concrete Structures; C. Standard: Beijing, China, 2015.
23. Sinha, S.; Routh, P.S.; Anno, P.D.; Castagna, J.P. Spectral decomposition of seismic data with continuous-wavelet transform. *Geophysics* **2005**, *70*, P19–P25. [[CrossRef](#)]
24. ASTM International. *ASTM E 1486 -Standard Test Method for Determining Floor Tolerance Using Waviness, Wheel Path, and Levelness Criteria*; ASTM: West Conshohocken, PA, USA, 2010.
25. ZRAPID. ZRAPID SLA 3D Printer. Available online: <http://www.zero-tek.com/en/sla880.html> (accessed on 1 August 2020).
26. Ram, A.; Jalal, S.; Jalal, A.S.; Kumar, M. A Density Based Algorithm for Discovering Density Varied Clusters in Large Spatial Databases. *Int. J. Comput. Appl.* **2010**, *3*, 1–4. [[CrossRef](#)]
27. Tang, P.; Akinci, B.; Huber, D. Quantification of edge loss of laser scanned data at spatial discontinuities. *Autom. Constr.* **2009**, *18*, 1070–1083. [[CrossRef](#)]
28. Fischler, M.A.; Bolles, R.C. Random Sample Consensus: A Paradigm for Model Fitting with Applications to Image Analysis and Automated Cartography. *Read. Comput. Vis.* **1987**, *24*, 726–740. [[CrossRef](#)]
29. Pratt, V. Direct least-squares fitting of algebraic surfaces. *ACM SIGGRAPH Comput. Graph.* **1987**, *21*, 145–152. [[CrossRef](#)]
30. He, Y.; Liang, B.; Yang, J.; Li, S.; He, J. An Iterative Closest Points Algorithm for Registration of 3D Laser Scanner Point Clouds with Geometric Features. *Sensors* **2017**, *17*, 1862. [[CrossRef](#)] [[PubMed](#)]
31. Li, F.; Kim, M.; Li, H. Registration-free 3D point cloud data acquisition technique for as-is BIM generation using rotating flat mirrors. In Proceeding of the 8th International Conference on Construction Engineering and Project Management, Hong Kong, China, 7–8 December 2020; pp. 3–12. Available online: <http://www.iccepm2019.com/wp-content/uploads/2020/12/Proceedings-of-ICCEPM-2020.pdf> (accessed on 12 December 2020).